

ROLE OF SEA SURFACE TEMPERATURE IN MODULATING LIFE CYCLE OF TROPICAL CYCLONES OVER BAY OF BENGAL

SHYAMA MOHANTY¹, RAGHU NADIMPALLI¹, KRISHNA K OSURI², SUJATA PATTANAYAK³,
U C MOHANTY^{1*} AND SOURAV SIL¹

¹*School of Earth Ocean and Climate Sciences, Indian Institute of Technology Bhubaneswar, Odisha, India*

²*Department of Earth and Atmospheric Sciences, National Institute of Technology Rourkela, Odisha, India*

³*National Center for Medium Range Weather Forecasting, Noida, Uttar Pradesh, India*

ABSTRACT

Sea surface temperature (SST) varies significantly in the presence of tropical cyclones (TCs). Using fixed SST throughout the integration of high resolution TC models is general practice in research and operational endeavor over the North Indian Ocean. The present study is to assess the impact of updating realistic SST in TC lifetime on track, intensity and rainfall of TCs. The Hurricane Weather Research Forecast (HWRF) model of single domain with 9km resolution is used. A total of 31 forecast cases are considered from 6 TCs during 2007–16 with unique track and intensity characteristics. A set of two numerical experiments are done without (CNTL) and with 6-hourly SST update (SST) in TC lifetime.

Mean track and intensity errors show that there is an improvement of 3–41% in track during 12–120h forecast length for SST run. The SST runs improve landfall position and time prediction by 20% and 33% respectively. The cross track error of SST run is comparable (44km) with average errors available for this basin (34km); and along track errors are improved by 60% as compared to CNTL as well as average errors of the basin. The model is biased to overestimate a weaker TC and underestimate a stronger TC, however, the bias is reduced in SST run by 5–51%. The analyses of wind, enthalpy flux and warm core structures provide insight for realistic intensity prediction of SST run unlike CNTL. Rainfall intensity and radial distribution is also improved in SST run. Thus, this study highlights the significance of ocean coupling with TC models to advance forecast guidance.

Keywords: tropical cyclone, HWRF, SST, Bay of Bengal

1. Introduction

Tropical cyclones (TCs) are one of the deadliest hydro-meteorological natural hazards formed over warm tropical and sub-tropical waters (Charney 1964). TCs over the North Indian Ocean (NIO) basins are not as gigantic as those in the other global basins. But the landfall of the TCs brings a lot of devastating impact on the coastal regions especially in the eastern coast of India because of its shallow bathymetry, funnel shaped architecture of coast line, low-lying delta areas associated with large number of river basins and highly dense population along the coast (Deo 2011, Dube 2009, Needham 2015). Therefore, accurate prediction of time and position of landfall of TCs and their intensity with longer lead time are very helpful to the people as well as the decision makers in the process of minimizing loss of life and property.

The enthalpy fluxes, known to be important for TC evo-

lution, are strongly influenced by sea surface temperature (SST) along with low level atmospheric temperature and moisture (Palmen 1948; Miller 1958; Riehl 1954). There is two-way interaction between SST and TC in its life cycle (Emmanuel 1986). Sharp changes in SST plays an important role in the intensity evolution of the TC (Kaplan and DeMaria 2003). For example, when TCs pass through warm waters, they tend to intensify (Shay et al. 2000; Goni and Trinanes 2003) and, conversely, TCs dissipate/weaken in the presence of cold waters (Ma et al. 2012).

Over the NIO region, high resolution mesoscale models have been used in the real time prediction of TCs using fixed SST during integration (Srinivas et al. 2013; Osuri et al. 2013; Mohanty et al. 2015; Nadimpalli et al. 2016; Osuri et al. 2017a). Considering model performance with such configuration, the track prediction is consistently better, however, the intensity prediction is still not good (Mohapatra et al. 2013a,b, 2017). This may be due to the facts that (i) SST is not updated during integration or lack of ocean cou-

Corresponding author: Prof. U C Mohanty, ucmohanty@iitbbs.ac.in

pling, (ii) lack of multiscale interactions, (iii) inadequate initial vortex information and (iv) constraint in using very high resolution numerical models involved in intensity prediction. In this study, we focus on SST interaction with TCs for improved prediction.

Many studies show that the SST changes in the presence of TC which in turn modifies TC intensity prediction (Schade and Emanuel 1999; Bao et al. 2000; Chan et al. 2001; Wu et al. 2007). Recent studies reported an improvement in the prediction of the TC intensity over the Atlantic basin by updating SST through ocean coupled model (Santabarria et al. 2013; Kim et al. 2014; Yablonsky et al. 2015) and over Pacific Ocean basin (Sandery et al. 2010; Jullien et al. 2014). Few studies over Bay of Bengal (BoB) show the significant impact of SST update on TC predictions over the BoB, particularly, the intensity evolution (Bongirwar et al. 2011; Mandal et al. 2007). A recent study over the BoB highlighted the ocean coupling in TC predictions and improvement is attributed to the realistic representation of SST (Srinivas et al. 2016). However, these studies are based on limited number of cases. Further, BoB is a warm ocean ($SST > 27^\circ\text{C}$; Bhat et al. 2004) round the year which is the pre-requisite condition for TC genesis and evolution (Gray 1975). Even after meeting the requisite of warm water, some TCs intensify and some dissipate over the BoB. Therefore, we hypothesized that the TC evolution depends on SST changes during lifecycle of a TC and the prediction of TC physical parameters (track, intensity and structure) can be improved through incorporation of realistic SST changes in the life cycle of TC.

In the present study, we have considered six TCs with different intensifications over the BoB during 2007 to 2016. Each case is a representative case of unique tracks observed during the time span. A total of 31 simulation cases are integrated at different initial times. The number of cases for each TC along with forecast period is given in the Table 1 with more specifications about the TCs. The brief details on uniqueness of these TCs are provided in the subsection 2.3.

2. Model, experimental design, data and methodology

2.1 HWRF modeling system:

HWRF is a high resolution coupled model developed at Environment Modeling Centre (EMC), National Centre for

Environmental Prediction (NCEP), designed with multi-nested moving domains and coupled for atmosphere, ocean and waves. The model is well suited for both single and parallel computing platforms. This fully compressible non-hydrostatic model is designed with a hydrostatic option (Janjic et al. 1994; Janjic 2010). Computation inside the model is done on a rotated longitude–latitude Arakawa E grid with 42 hybrid (terrain following pressure sigma) vertical coordinates. The model uses rotated lat-lon projection that minimizes the convergence over the meridian. Table 2 summarizes the model specifications and various options of physics and dynamics of HWRF model used in the present frame-work.

HWRF modelling system is based on the combination of specially designed physics schemes to best predict the hurricane (Gopalakrishnan et al. 2010). The Geophysical Fluid Dynamics Laboratory (GFDL) long-wave and short-wave radiation schemes are incorporated in the model along with the cloud microphysics effects. It has a well-tested NCEP Global Forecasting System (GFS) scheme for planetary boundary layer parameterization (Hong and Pan 1996). The Simplified Arakawa-Schubert scheme is used for cumulus parameterization. (Arakawa and Schubert 1974; Grell 1993).

2.2 Experimental design and data used

The HWRF model with a static domain of 9 km resolution is considered with east-west extension of 190 points and north-south extension of 350 points, with the latitudinal extension from 0° N to 24° N and longitudinal extension from 76° E to 96° E. The physics module of HWRF system follows India Meteorological Department (IMD) operational setup (Das et al. 2016; Osuri et al. 2017a). Two sets of numerical experiments are conducted, the first set is done with initial and boundary conditions (IBCs) from Global Forecasting System (GFS) of National Center for Environmental Prediction (NCEP) along with Reynolds SST (known as CNTL); and the second set is carried out with the updating of daily Real Time Global (RTG) SST (RTG-SST) data, hereafter referred as SST experiment (SST). Some previous studies have been conducted using a three-day composite Tropical Rainfall Measuring Mission Microwave Imager SST (TMI-SST) for updating SST to the model, but failing to represent realistic SST fields in

TABLE 1. Details of all cases simulated with nature and synoptic conditions

Name	Simulation period in 12h intervals (total no. of forecast)	Observed Landfall time and location	Nature	Intensity
Sidr	1200 UTC 11 – 0000 UTC 15 Nov 2007 (7)	1600 UTC 15 Nov (Bangladesh)	Recurved	ESCS
Nargis	1200 UTC 29 Apr – 1200 UTC 02 May 2008 (7)	1400 UTC 02 May (Myanmar)	Recurved	ESCS
Viyaru	0000 UTC 11 – 1200 UTC 12 May 2013 (4)	0800 UTC 16 May (Bangladesh)	Recurved	CS
Phailin	1200 UTC 09 – 1200 UTC 11 Oct 2013 (5)	1700 UTC 12 Oct (Odisha)	Straight	ESCS
Madi	1200 UTC 09 – 0000 UTC 11 Dec 2013 (4)	1700 UTC 12 Dec (Tamilnadu)	Recurved	VSCS
Roanu	0000 UTC 18 – 1200 UTC 19 May 2016 (4)	1000 UTC 21 May (Bangladesh)	Recurved	CS

TABLE 2. HWRF model configuration details used for present study

Model Options	Specifications
Dynamic Core	Non-hydrostatic Meso-scale Model (NMM)
Vertical Levels	43
Projection	Rotated latitude-longitude
Horizontal Grid Type	Arakawa E-grid
Time Integration Scheme	Horizontal: forward-backward scheme
Vertical: implicit scheme	
Horizontal Advection	Adams-Bashforth Scheme
Initial and Lateral Boundary Condition	GFS analysis and forecast products
Resolution	9 km
Domain Extent	190 (East-West) 350 (North-South)
Microphysics Schemes	Ferrier scheme (Ferrier 1994; Ferrier et al. 1995)
Longwave radiation	Modified GFDL (Kurihara et al. 1998)
Shortwave radiation	Modified GFDL (Kurihara et al. 1998)
Surface layer	Monin-Obukhov similarity theory (Kurihara and Tuleya 1974; Kurihara et al. 1998)
Planetary boundary layer	NCEP GFS nonlocal scheme (Janjie 1994)
Land surface module	GFDL slab scheme (Tuleya 1994; Kurihara et al. 1998)
Cumulus parameterization	Simplified Arakawa-Schubert scheme (Pan and Wu 1995)

the model (Bongirwar et al., 2011; Mandal et al. 2007). To overcome the drawback of TMI-SST datasets, RTG-SST with resolution $0.5^\circ \times 0.5^\circ$ have been used. Thus, the SST experiments are carried out with incorporation of RTG-SST daily to the model. All the cases of cyclones are simulated to create both CNTL and SST forecasts. The present work is carried out with the atmospheric component of the modeling system. The above-mentioned model configuration is integrated for a total of 31 cases from 6 cyclones with different initial conditions (ICs). The forecasts are produced from 120 h to 24 h with reference to landfall time. Note that each simulation ends after 12 h of landfall time.

6-hourly GFS analyses and forecast products are used as initial and boundary conditions (BC) respectively in the present study. Daily RTG-SST of the NCEP (Reynolds 1988; Thiébaux 2003) are used. The detailed synoptic conditions and best track data for these 6 TCs are obtained from Regional Specialized Meteorological Center (RMSC), IMD (http://www.rsmcnewdelhi.imd.gov.in/index.php?option=com_content&view=article&id=167&Itemid=502&lang=en). The multiplatform satellite surface wind analysis developed at Cooperative Institute of Research in the Atmosphere (CIRA), Colorado University, USA (Knaff and DeMaria 2006) is used to verify model predicted TC structures.

2.3 Tropical cyclone cases selected for the study

The synoptic conditions associated with the TCs considered in this work are briefed in this sub-section.

2.3.1 Extremely Severe Cyclonic Storm (ESCS) Sidr

With very high favorable conditions of moderate upper-level wind shear and developing convection for genesis of TC over southwest BoB and adjoining south Andaman Sea during 8–10th November, 2007, a low pressure system was generated at 0300 UTC of 11th November. Rapidly, it concentrated into a depression and then deep depression on the same day. It further intensified into a cyclonic storm (CS; maximum 10m sustained wind: 34–47 knots), named Sidr at 0300 UTC of 12th November about 220 km southwest of Port Blair. The conducive conditions further made the system into a severe cyclonic storm (SCS; maximum 10m sustained wind: 48–63 knots) at 1200 UTC and very severe cyclonic storm (VSCS; maximum 10m sustained wind: 64–89 knots) at 1800 UTC steering the system in north-northwestward direction. Further intensifying into an ESCS (maximum 10m sustained wind: 90–119 knots) and continuing in northward direction, the TC crossed Bangladesh coast around 1700 UTC, about 100 km south of Dhaka. Although the system rapidly lost its strength after landfall, it could bring strong and a lot of rain causing huge life and property loss.

2.3.2 ESCS Nargis

A low-pressure system originated over southeast BoB at 0300 UTC of 27th April, 2008 under positive circumstances for cyclone formation, intensified into a CS Nargis at 0300 UTC of 28th April and into a VSCS at 0300 UTC of 29th April. The system recurved northwestwards after moving northwestward initially. The storm continued to intensify even after recurvature due to its encounter with a warm core eddy underneath. It made landfall on southwest coast

of Myanmar between 1200 and 1400 UTC of 2nd May. As the storm maintained the intensity of CS about 12 h after the landfall, it brought about extensive loss of life and property.

2.3.3 CS Viyaru

The cyclone Viyaru originated as a low-pressure disturbance in lower latitude near 5° N at 0900 UTC of 10th May 2013. It made recurvature northeastwards after northwestward movement. It crossed Bangladesh coast about 30 km south of Feni around 0800 UTC 16th May. The sustained maximum wind during the time of landfall was about 85–95 kmph. It moved very fast about 40–50 km per hour on the day of landfall for which the loss after landfall was relatively less.

2.3.4 VSCS Phailin

TC Phailin originated from a remnant cyclonic circulation from the South China Sea. It formed as a low pressure on 6th October over Tenasserim coast and intensified into a well mark low pressure in 7th October over north Andaman Sea which later concentrated into a deep depression over the same region on 8th October. It moved west-northwestwards and intensified into a cyclonic storm on 9th morning Indian Standard Time and later intensified into severe cyclonic storm and then rapidly intensified to very severe cyclonic storm in the forenoon of 10th October. It crossed Odisha coast and adjoin Andhra Pradesh coast near Gopalpur (Odisha) around 2230 h IST of 12th October causing extremely heavy rainfall over Odisha leading to floods (Osuri et al. 2017a).

2.3.5 VSCS Madi

In the morning of 6th December, 2013, a depression formed over southwest BoB and became deep depression with very slow movement of northward intensifying into a CS Madi on morning of 7th December. It strengthens into SCS in the forenoon of 8th December. With the entrainment of cold air, passage on colder ocean and increasing vertical wind shear, the VSCS Madi began losing its strength becoming a SCS in the evening of 9th December. The weakening system moved southwestward after reaching the latitude of 15.7° N under the influence of lower and middle tropospheric steering ridge. The continued weakening system became deep depression to depression during the night of 11th December and crossed Tamil Nadu coast near Vedaranniyam around 1330 UTC of 12th December and emerged into Palk strait around 1500 UTC and again crossed Tamil Nadu coast near Tondi around 1700 UTC. It possessed a unique track with recurvature in southwestwards.

2.3.6 CS Roanu

TC Roanu developed over southwest BoB near Sri Lanka coast during 14th May 2016 moving northeastwards and intensified slowly. Nurturing under conducive conditions

to strengthen, it continues to move towards northwestward skirting Tamil Nadu and Andhra Pradesh coast and concentrated into a CS over west-central BoB at 0000 UTC of 19th May. It continued to move along the east coast of India with a maximum sustained speed reaching 40 knots at 0600 UTC of 19th May and 45 knots at 1800 UTC of 20th May. Then the system sustained its strength continuing skirting along the coast and made landfall on Bangladesh north to Chittagong around 1000 UTC of 21th May as CS. It took a unique path (first time over the basin) moving closely along the east coast of India and recurred northeastwards travelling about 2300 km.

3. Results and discussion

Different statistical and structural analyses have been carried out for all the cases. The error and skill metrics are provided as the mean values of all the cases. However, two cases; TC Viyaru and TC Phailin are selected as representative cases following the intensity and season of formation for diagnosing the results.

3.1 SST data verification and initial impact of SST

The RTG-SST data used in the present study have been verified against buoy observations over BoB basin along with the TMI-SST analysis. These SST products are validated at various buoy locations in both pre-monsoon and post-monsoon seasons during the period 2005–2013 and presented in Figure 1a and 1b respectively. The analysis shows the correlation of RTG in pre-monsoon season is 0.98 whereas for TMI-SST, correlation is 0.46. For post-monsoon season, the correlation value is about 0.24 for RTG-SST but TMI has the value 0.38. The RMSE of TMI is larger than that of RTG in both pre- and post-monsoon seasons. Bias of RTG-SST indicates that RTG is overestimated by 0.3°C whereas TMI underestimates SST by 1.3°C in pre-monsoon season. In post-monsoon season, RTG has a little underestimation (0.05°C) while TMI has larger overestimation of the SST (0.7°C). Therefore, by considering the above results, RTG-SST analysis is selected over TMI-SST as the ocean boundary condition in SST experiments.

The operational model set-up takes Reynold's SST as input (used as input to CNTL experiments in the present study) which is a 7-day averaged data. Hence, inter-comparison between RTG-SST and Reynold's SST is performed with respect to Buoy data at the closest buoy location to the TC passage. Buoy BD09 (latitude: 17.9, longitude: 89.7) and BD10 (latitude: 16.48, longitude: 88.0) are chosen for TC Viyaru and TC Phailin respectively. Figure 2 shows the variation of SST from Reynold's SST, RTG and Buoy SST at above stated Buoy locations during the TC lifetime for Viyaru and Phailin. As Reynold's SST is a 7-day averaged SST, the variation in SST due to TC interaction with upper ocean is not captured. RTG-SST compared to buoy data in Figure 2, reflects the variation of SST as that of Buoy data but with an overestimation of 0.08° to 0.8°. Figure 3 shows

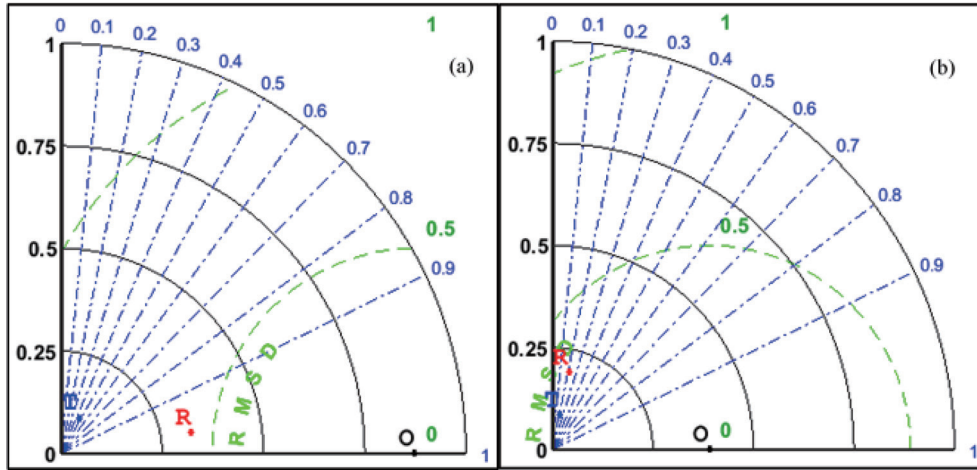


FIG. 1. Validation of RTG and TMI SSTs against buoy observations at 9 locations over BoB for (a) pre-monsoon period and (b) post-monsoon period

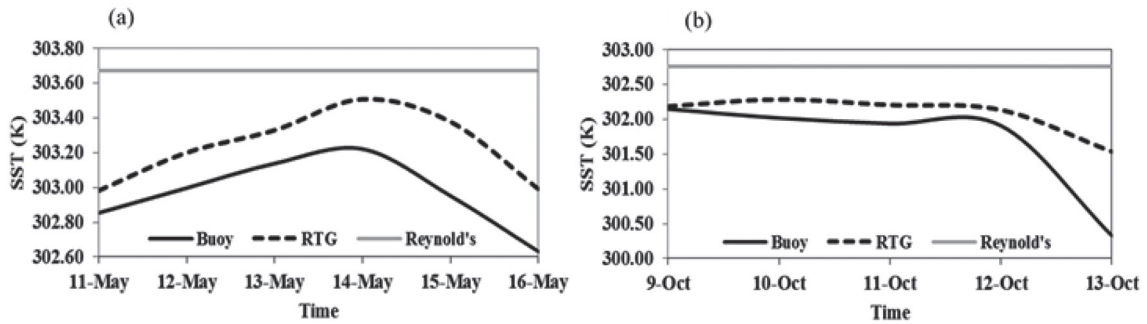


FIG. 2. Comparison of SST change from Buoy, RTG and Reynold's data at Buoy locations before, during and after the passage of (a) TC Viyaru and (b) TC Phailin

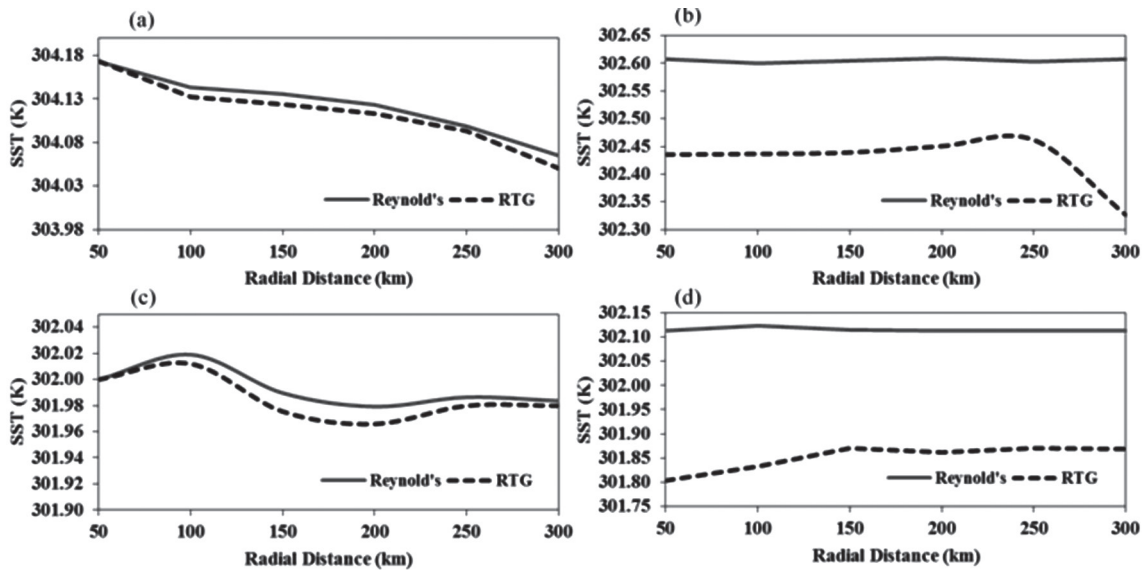


FIG. 3. Radial SST variation for CNTL and SST updated experiments at initial and peak intensity time for (a, b) TC Viyaru and for (c,d) TC Phailin respectively

the radial variation of SST at initial and peak intensity time of TC Viyaru and TC Phailin from Reynold's SST input and RTG-SST input to the model. Although the initial SSTs as input to the models for both the experiments are similar with radial structure with less value of SST for RTG, there is notable difference of the same at the peak intensity shown in Figure 3c and 3d for TCs Viyaru and Phailin where the difference rises up to 0.3 K. The SST variation introduced through RTG-SST has potential to modify the structure and intensity during the TC lifecycle, thus RTG has been chosen for the experiments.

3.2 Statistical analysis of model forecast

The averaged model generated SSTs for both CNTL and SST run at different forecast hours are plotted in Figure 4. As the model is forced with constant SST for CNTL runs, the SST does not change with time for CNTL runs. But, the real time SST forcing in SST runs could generate the SST variations for which the domain averaged SST with respect to time gradually decreases (shown in Figure 4), may be due to the cooling happens from strong winds.

3.2.1 Track and intensity error

The track and intensity guidance are the essential parameters for the disaster management authorities. Figure

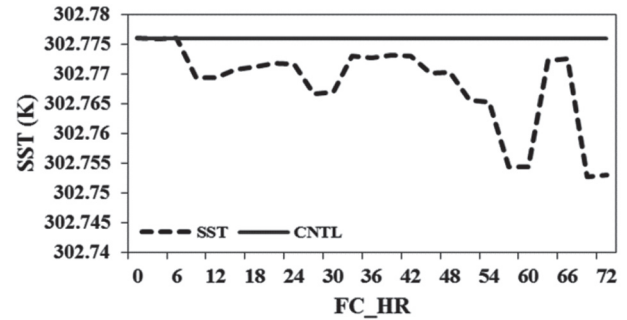


FIG. 4. Model SST variation for CNTL and SST updated experiments averaged over all 72 hour forecasts

5 provides the track simulations for all the TCs along with IMD best track. The tracks are shown with circles of maximum average error over all ICs at 0, 24, 48, 72, 96 and 120 h simulation length. Higher the radius, larger the track error. Although the tracks from SST and CNTL experiments appears to be similar, the position error is found to be less in case of SST simulations. It is noticed that most of the times, the errors are increased with increase in forecast hours. The radii of error circles are reduced for each SST simulation demonstrating better performance of the

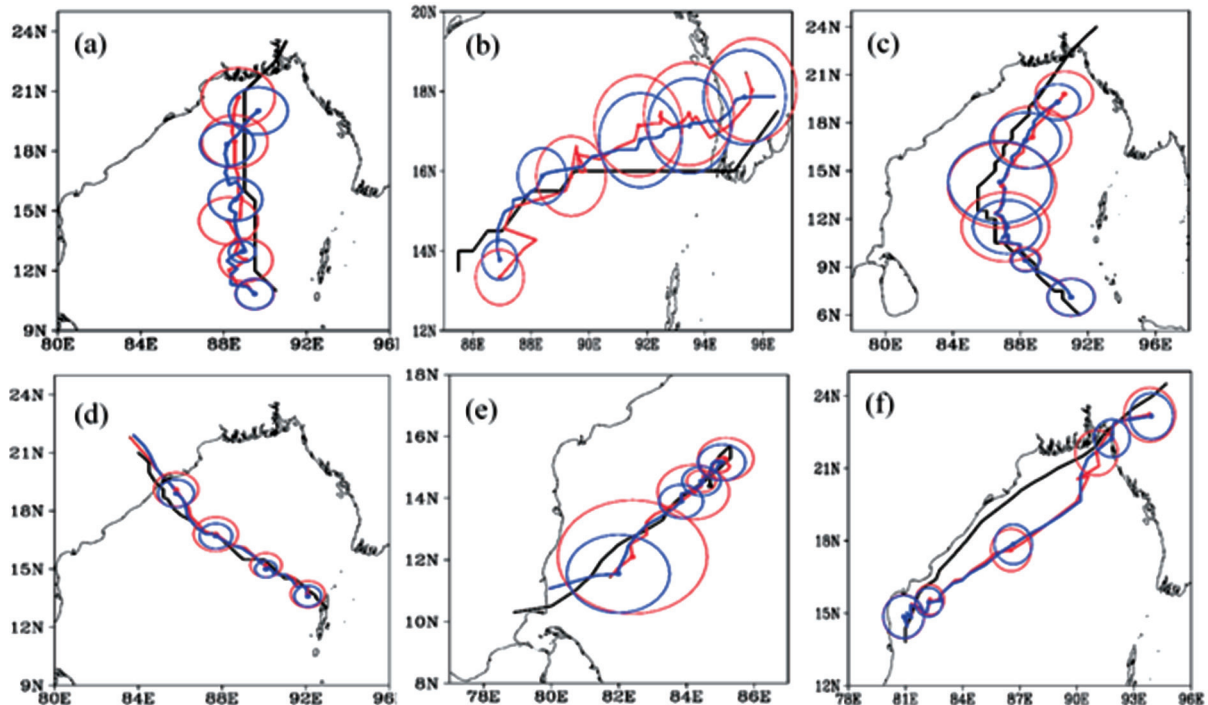


FIG. 5. Tracks of all cyclones simulated for CNTL (red), SST (blue) experiments with first ICs compared to IMD best prediction (black). The red and blue circles are the averaged position errors at 0, 24, 48, 72, 96 and 120th hours of CNTL and SST experiments respectively, calculated for all ICs. The figures are for (a) Sidr,(b) Nargis, (c) Viyaru, (d) Phailin, (e) Madi and (f) Roanu.

respective experiment in prediction of tracks. Out of the six cyclone cases, Phailin has the least track error with reduced value in SST case.

Further, the model predictions are evaluated calculating directionality errors for tracks such as along track (AT), cross track (CT) errors and direct position error (DPE). CT and AT errors give idea about whether the model forecasted position is to right or left of the best-predicted position and whether the TC is moving faster or slower respectively. The calculation of CT and AT are explained in Fiorino et al. (1993) and Osuri et al. (2013). Figure 6a and 6b show the CT and AT errors for CNTL and SST experiments respectively, averaged over all 31 cases. The overall CT error has mostly negative values depicting the model track has a leftward bias for CNTL simulations. However, the bias is reduced in SST experiments for longer forecast hours. A comprehensive statistical analysis by Osuri et al. (2013) shows that CT and AT errors for 72 h forecast from 9km Weather Research Forecast (WRF) Advanced Research WRF (ARW) model simulated for 100 cases of TCs over BoB are 34 km and -104 km respectively (Osuri et al. 2013). CT error for CNTL and SST run for 72 h are -79 km and 44 km respectively matching of CT error for SST run with the previous study conducted for 100 TCs over BoB. Similarly, AT errors for CNTL and SST simulation for 72 h are -45 km and -77 km respectively, show closer value for SST runs compared to the previous study discussed here. More negative value of AT error in case of SST simulation shows slower movement of the TCs. This can be attributed to the passage of TC over colder SST introduced because of TC interaction in SST runs (Zhao et al., 2016). DPE is the vector displacement between the observed (best estimated position) and the model estimated position at a particular time. Figure 6c shows the average DPE at different forecast hours. DPE error is reduced for SST runs as compared to CNTL run. There is more improvement in track at longer forecast hours.

Average mean absolute error (MAE) and mean bias of intensity in terms of 10m maximum sustained wind for CNTL and SST simulations are shown in Figure 6d and 6e respectively. Intensity errors in terms of MAE are less and similar in both the experiments for shorter forecast hours (<72 h) and, thereafter the error decreases significantly in SST run when compared to CNTL run. Significantly less error is observed at 120 h but with less number of sample size. However, 60 h forecast gives the least error for both CNTL and SST runs. Similarly, RMSE calculated (not shown in Figure) follows the same with less error for SST runs. Figure 6e shows the mean bias of 10m wind. Positive (negative) value indicates overestimation (underestimation) of the intensity. It is noted that the bias is reduced considerably at longer forecast length (>72 h) in SST run as compared to CNTL run. Overestimation of intensity in CNTL run could be attributed to the higher SST throughout the integration. It is known that higher the SST higher the

intensity (Zhao et al. 2016). In case of the SST run, the SST decreases during life cycle of TC due to upwelling of colder water and rainfall (Dare et al. 2011). In comparison of track and intensity improvement, the SST experiments illustrate greater percentage of improvement compared to CNTL experiments. Mean intensity bias shown in Figure 6e indicates up to 72 h of forecast where sample size is considerably larger, model has positive bias with reduced error for SST runs. With relatively smaller sample size for 96 h and further with less number of cases for 120 h, there is large underestimation of wind forecast with decreased error for SST simulations. The 6-hourly percentage improvement in both track and intensity are shown in Figure 6f. There is 3-41% of improvement in overall track prediction and 5-51% of improvement in overall intensity prediction from 24 h to 120 h forecast period. Till 3 days of forecast, the intensity skill improvement lies within 10% whereas the skill improves to 40% for 108 h forecast. Hence the statistical analysis shows SST runs can improve the track and intensity of TCs with a minimum of 3 days lead.

The skill of the model is calculated with respect to intensity stage at the time of model initialization is presented in Figure 7. The skill of SST run is noticeably higher when the model is initialized at deep depression and CS stages. The skill of CNTL and SST runs slowly decreases and becomes same as the TC intensifies to SCS and above categories at the time of initialization. It may be concluded that the incorporation of SST changes during TC lifetime has significant impact on intensity during initial intensity stages of the TCs.

3.2.2 Landfall error

Considering all the cases which have made landfall, the error statistics for landfall position and time error are evaluated and presented in the Table 3. It shows that for longer forecast hours the error is larger, similarly, error is less for shorter forecast hours except at 36h. SST simulated runs consistently give less position and time errors as compared to that of CNTL run. Landfall time error for SST cases is less than that of the CNTL cases for all forecast hours, thus shows further slower movement of the storm in case of CNTL as compared to SST simulations. The improvement in landfall position and time error can be explained from the improved CT and AT errors in SST runs. Mean position and time error calculated for CNTL are 114 km and 6h respectively whereas mean position and time error for SST are 92 km and 4 h respectively.

3.3 Structural characteristics and diagnostics

In order to see the associated processes that helped in improving the TC prediction with SST experiments, the horizontal and vertical structures of horizontal winds, surface enthalpy flux and warm core are analyzed for all the TC cases. However, two representative cases having unique intensity evolution have been chosen – Viyaru (initialized at 12 UTC 11th May 2013) and Phailin (initialized at 12

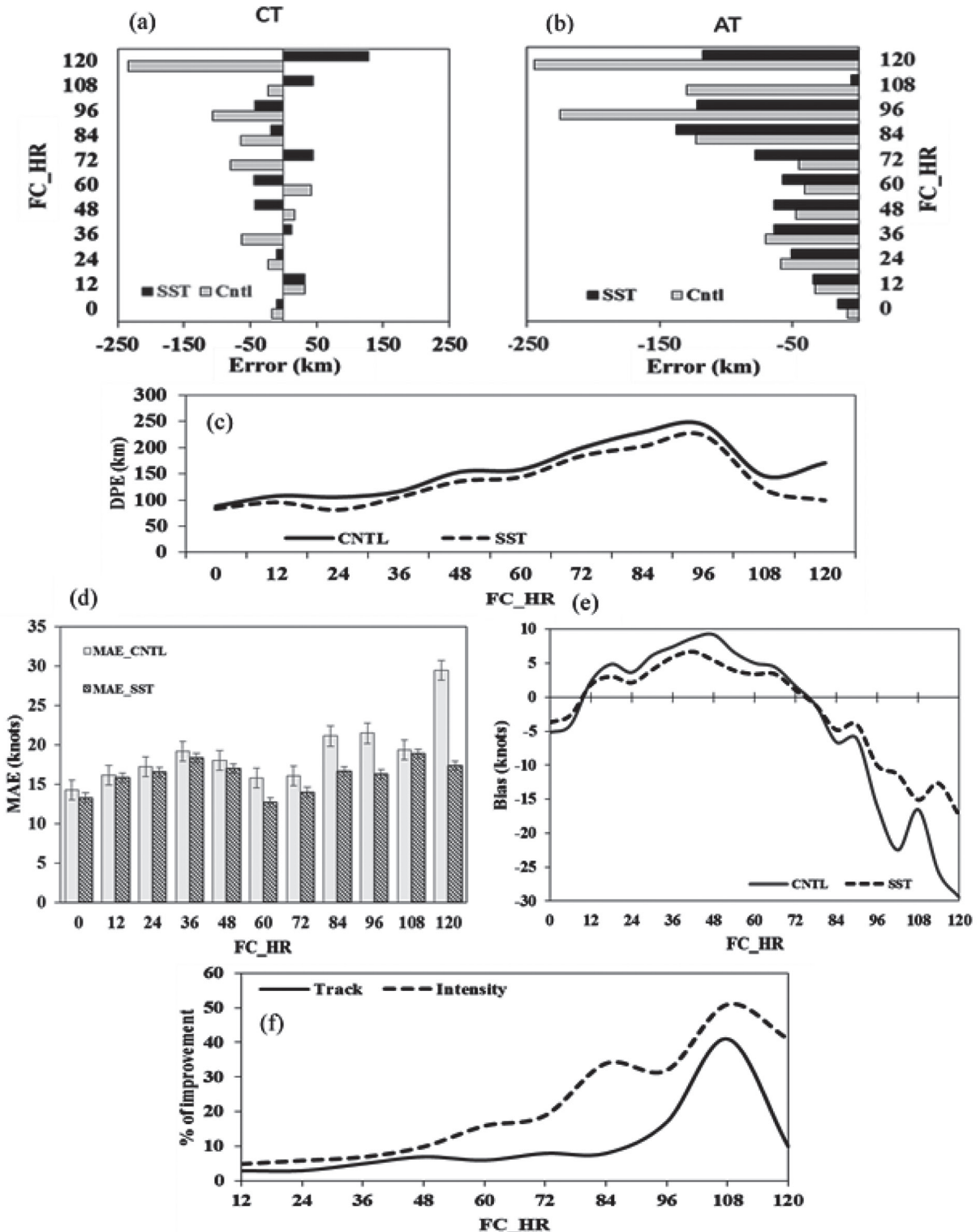


FIG. 6. Average track error of all 31 cases from 6 simulated cyclones for CNTL and SST experiments at different forecast hours; panel (a) shows cross track error (CT) and (b) along track error (AT), (c) direct position error (DPE). (d) shows average mean absolute error (MAE) and (e) shows mean bias computed for all 31 cases from 6 cyclone for respective CNTL and SST simulated intensity in terms of 10m maximum wind. The overall % of improvement in track and intensity prediction with respect to forecast hour is shown in (f).

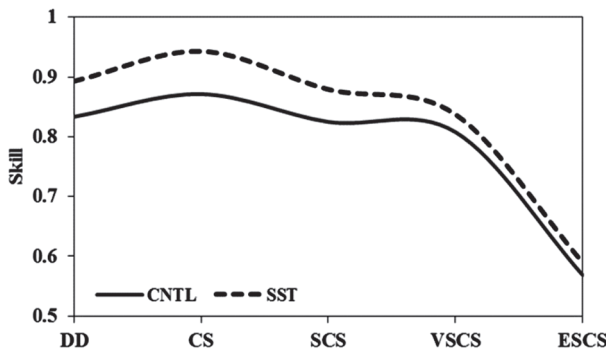


FIG. 7. Skill score for predicting different intensity of TC for CNTL and SST experiments

UTC 9th October 2013).

3.3.1 Wind analysis

The model simulated horizontal cross-section of surface winds of two cases at the maximum intensity are shown along with observed satellite derived winds (http://rammb.cira.colostate.edu/products/tc_realtime) in Figure 8. According to satellite wind analysis and synoptic observations, TC Viyaru was at CS stage ($34 \leq CS \leq 47$). There is overestimation (50 knots) of the winds at the peak intensity (at 12 UTC 15th May 2013) of TC Viyaru as simulated from CNTL (Figure 8b). In the SST experiment, TC intensity was realistically predicted (35 knots) as that of the observation. Considering TC Phailin, satellite analysis indicated a symmetric vortex of 110 knots (Figure 8d) at 06 UTC 12th October which is reasonably well replicated in SST run with maximum winds of 95 knots in the right side of the vortex (Figure 8f). However, the CNTL run could show similar intensity, the 95 knots winds are not replicated well (Figure 8e). The SST run could generate more symmetric vortex, close to satellite analysis.

Vertical cross-section of horizontal winds gives clear idea about the vortex. Vertical distribution of horizontal winds at the peak intensity of both the TCs are shown in Figure 9. The results show the vertical cross section of the winds with contours of CS and SCS winds (17 and 34 m/s respectively) for the two cyclones at mature stage. From Figure 9a, the CNTL-simulated vortex is stronger with SCS winds

extending from surface to 500 hPa in the left quadrant and up to 200 hPa in the right sector of Viyaru whereas in SST run, the vortex is weaker as compared to CNTL. The results also show the radius of maximum wind is less in CNTL as compared to SST run. The weaker vortex or less intense storm in SST run is mainly due to the SST cooling experienced due to the passage of Viyaru. Pothapokala et al. (2017) showed a cooling of 3°C during the passage of slow-moving TC, Viyaru. For TC Phailin, stronger and more symmetric winds are extended from surface to upper level for CNTL and SST runs. A well-defined TC center is noticed with less winds ($<10 \text{ ms}^{-1}$) in SST run and consistent with the known fact that wind is calm or minimum at the center. However, winds are relatively high ($>20 \text{ ms}^{-1}$) in CNTL run as compared to SST run in the TC center.

3.3.2 Flux analysis

The enthalpy flux is one of the principal parameters of air-sea interaction during the passage of the storm over ocean. This flux provides additional energy to the TCs leading to evolution, maintenance and sudden change in intensification processes (Mandal 2007; Bell and Montgomery, 2008; Lin et al., 2009; Chen et al. 2013; Osuri et al. 2012a). The spatial distribution of enthalpy flux is shown in Figure 10 for both the representative TCs. The satellite picture of Viyaru (Figure 10a) shows the system is not well developed lacking a clear eye, having thicker convective cloud at the right rear quadrant. Corresponding to this cloud structure, both experiments showed maximum enthalpy flux in the similar quadrant. However, the magnitude of flux is more in CNTL run (700 W/m^2 to south of the vortex) which could be responsible for the overestimation of intensity. However, SST run could show less enthalpy flux ($<550 \text{ W/m}^2$) which can be attributed to realistic SST input. Considering TC Phailin, the satellite imagery shows that the convective bands are symmetrical and maximum convection lies in the right rear quadrant of the vortex. The enthalpy structure in SST run is more symmetric with maximum enthalpy ($>1200 \text{ W/m}^2$) in the right rear quadrant. But CNTL did not show similar structure. It is to be noted that the spatial distribution of the enthalpy flux lies inside the cyclonic wind contour where strong flux exchange occurs to feed the system.

The enthalpy flux is calculated in the TC core ($1^\circ \times 1^\circ$ box) during the life cycle of the TCs and presented in

TABLE 3. Landfall error metrics calculated over all landfalling cases

FC_HR	CNTL_Position	SST_Position	CNTL_Time	SST_Time
84	169.5	144.5	-7.0	-4.0
72	188	160	-5.5	-3.5
60	77	60	-4.5	-4.0
48	95	63	-8.0	-7.0
36	109	91	-5.5	-4.0
24	73	56	-5.0	-2.0

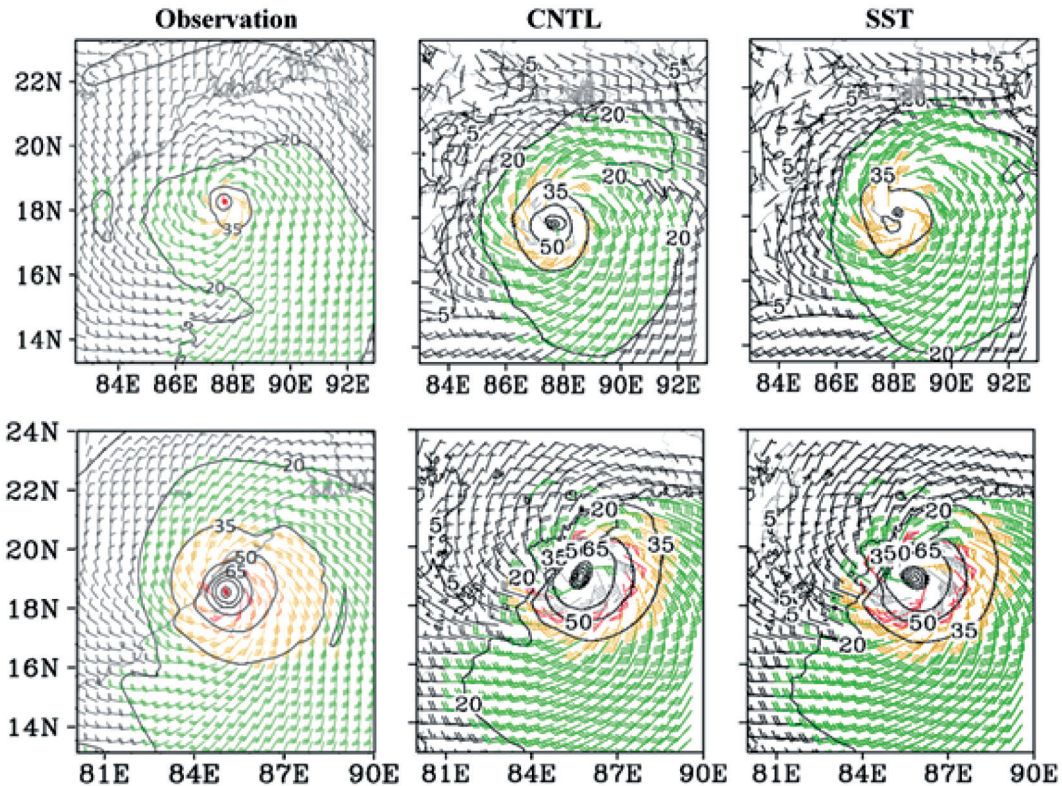


FIG. 8. Wind structure for (a) CNTL, (b) SST experiments and (c) satellite wind surface analysis observation for cyclone Viyaru at peak intensity time for cyclone Viyaru. (d-e) are same as (a-c) but for cyclone Phailin.

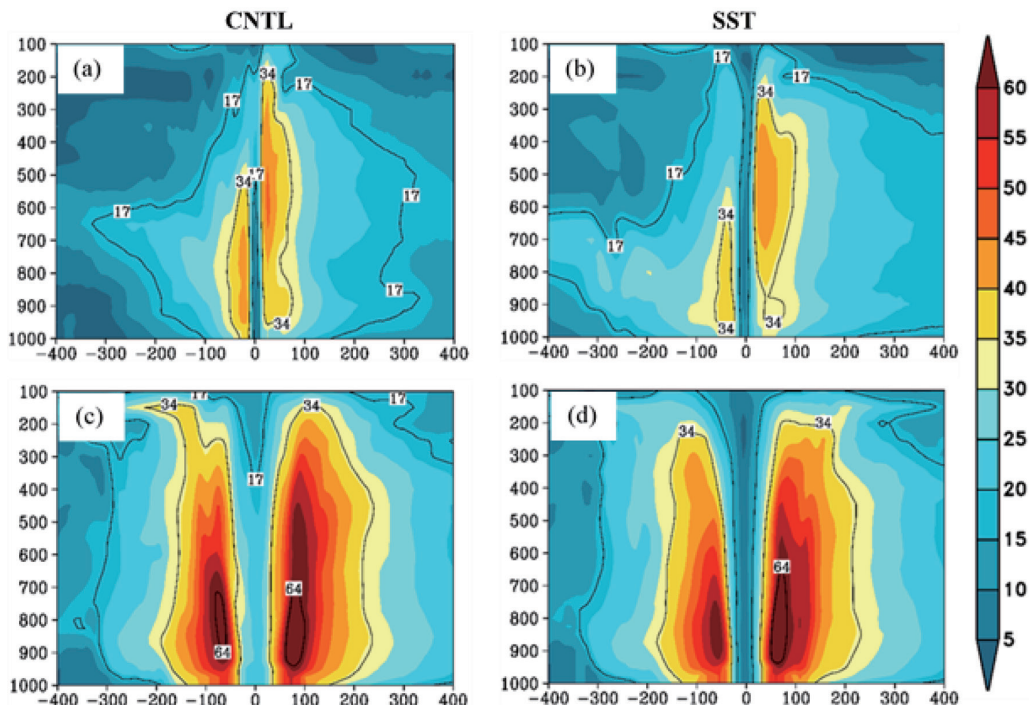


FIG. 9. Zonal vertical cross-section of horizontal wind at peak intensity for (a) CNTL and (b) SST experiments for cyclone Viyaru. 2nd panel (c,d) is same but for cyclone Phailin

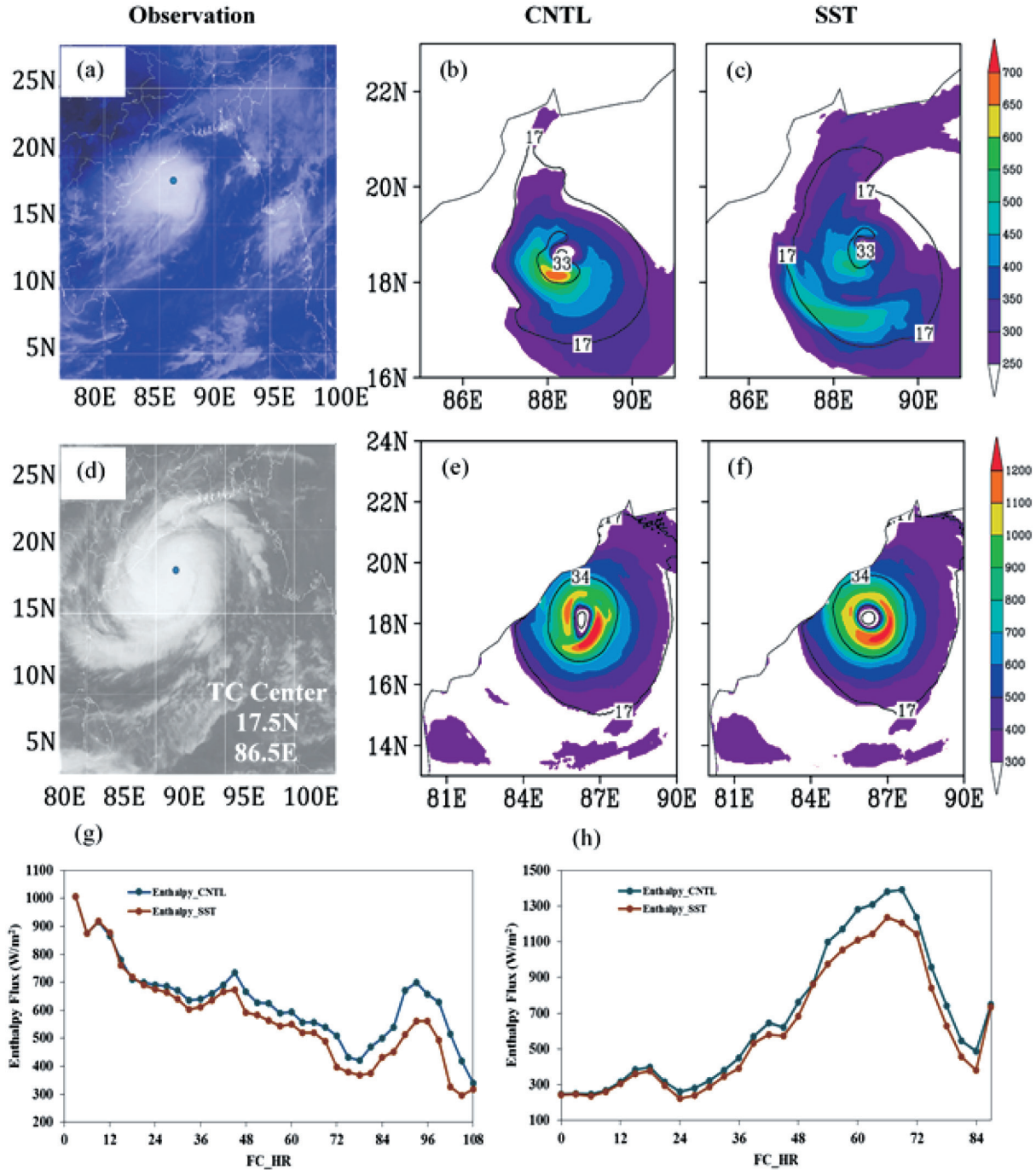


FIG. 10. Simulated enthalpy flux at peak intensity from (b) CNTL and (c) SST experiments for Viyaru along with (a) Infrared satellite image for qualitative comparison. (e-f) are same as (b-c) for Phailin as with (d) visible imagery for comparison. Time series of enthalpy flux averaged over TC core ($1^\circ \times 1^\circ$) for (g) Viyaru and (h) Phailin.

Figure 10g and 10h for Viyaru and Phailin respectively. The enthalpy flux is consistently smaller for SST runs as compared CNTL runs. For TC Viyaru, the flux difference between CNTL and SST runs is more after 24 h forecast and is mainly due to the fact that TC Viyaru is a slow moving

TCs. It is known fact that slow moving TC produce more cooling during its passage (Pothapokala et al. 2017). This cooling is reflected in SST run with less enthalpy flux. In case of Phailin, the difference between the runs is less except during peak intensity time (48-72 h forecast period).

The reduced enthalpy flux in SST run is attributed to realistic SST cooling due to stronger TC winds at peak time (Gao et al. 2016). Hence it can be inferred that the CNTL simulation fails to count the cooling associated with the storm and gives higher enthalpy flux, leading to overestimating the intensity.

3.3.3 Vertical thermal structure analysis

Figure 11 shows the radial height cross section of the temperature anomaly at peak intensity for both the experiments and compared with the satellite analysis available at (http://rammb.cira.colostate.edu/products/tc_realtime/). Previous studies from Chen and Gopalakrishnan (2015), Nadimpalli et al. (2016) and Osuri et al. (2017a) have discussed the role of upper level warm core in the TC intensification. From the satellite analysis of TC Viyaru, positive temperature anomaly of $\sim 1^{\circ}\text{C}$ in the middle to upper levels (4–8 km height) extending up to 200 km radial distance from TC center and a negative temperature anomaly of 1.5°C at the height of 12 km are noticed. Unlike the observation, negative temperature anomaly at the upper atmosphere (~ 12 km) could not be produced by both CNTL and SST runs. However, the CNTL run shows two maxima of positive anomaly of $\sim 7^{\circ}\text{C}$ at 6 km height and 6 km at 12 km height. In contrast, SST run could show warm core of higher intensity ($\sim 6^{\circ}\text{C}$) at 6 km height only. Like in satellite analysis, the SST run could show relatively cooler anomalies (4°C) at 12 km height. The two warmer core maxima in CNTL might have supported for the over-

estimation of intensity as compared to the observed storm. The comparable structure of temperature anomaly in SST run explains more realistic evolution of intensity as compared to CNTL run. In the case of Phailin (Figures 11d, 11e and 11f), a very strong warm core is observed with a temperature anomaly of 8°C near 12–13 km of height. In CNTL run, stronger warm core (10°C) is formed at 12–14 km of height whereas SST run could produce a temperature anomaly of 9°C at a height of 10–13 km being closer to observation. Also, the radial extension of the maxima is comparable to the observation in SST run.

3.4 Rainfall analysis

The heavy rainfall associated with TCs is one of the crucial parameters which set potential damages to the livelihood. Hence, the rainfall guidance during landfall in advance is important for disaster management and mitigation activities. The Figure 12a shows spatial rainfall from CNTL and SST runs compared with IMD-Tropical Rainfall Measuring Mission (TRMM) merged rainfall in the day of landfall. The TCs making landfall with CS or higher intensity are considered in this analysis, hence TC Madi and Roanu are excluded. According to RMSC report (2014), Madi could not produce heavy rainfall over land whereas Roanu brought extremely heavy rainfall (~ 35 cm) over Tamil Nadu and Andhra Pradesh during its deep depression stage but could not shower heavily during landfall (RMSC 2016). In case of TC Sidr (Figure 12a), rainfall in

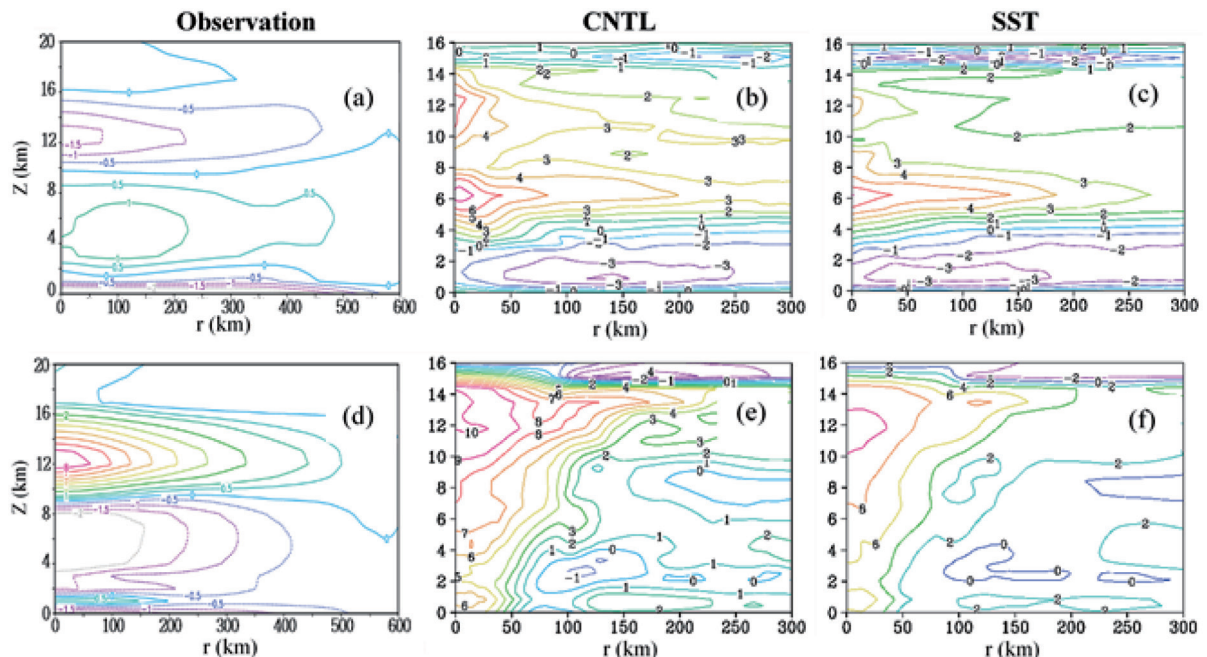


FIG. 11. Radial distribution of temperature anomaly at peak intensity for (a) satellite derived product, (b) CNTL and (c) SST experiments for cyclone Viyaru valid at 12 UTC 15 May 2013. 2nd panel (d,e,f) is same but for cyclone Phailin valid at 06 UTC 12 October 2013.

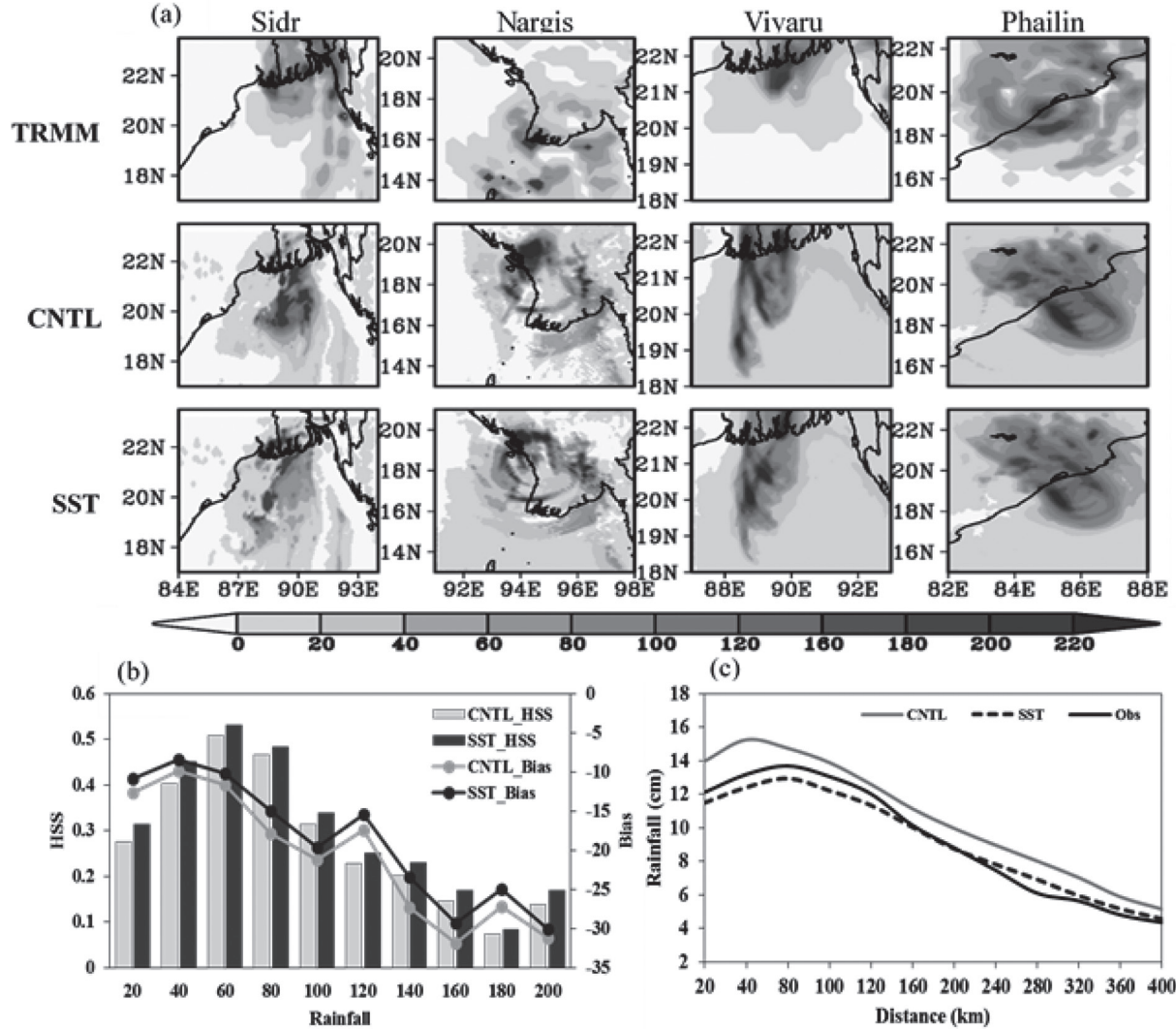


FIG. 12. (a) Spatial pattern of 24-h accumulated rainfall for the simulated cyclones on the day of landfall. First row provides TRMM rainfall for Sidr, Nargis, Viyaru and Phailin. Second row and third row are same as first row but for CNTL and SST runs respectively. (b) shows mean skill scores (HSS and mean bias) calculated for different rainfall categories and (c) mean radial distribution of rainfall from CNTL and SST experiments along with IMD observation.

the coastal region is well replicated in SST run than CNTL run. CNTL run produced excess rain over ocean whereas as rainfall predicted by SST run is less than that of CNTL. In both the runs, the rainfall over the Bay is overestimated. However, eliminating the higher rainfall patch near 20°N latitude and 88°E longitude, SST run could produce the realistic rainfall pattern and intensity as observed. With a careful analysis, one can notice that near the position of 22°N latitude and 90.5°longitude, CNTL run fails to produce the rainfall patch, but SST run could generate comparable amount of rainfall as observed. In case of Nargis, CNTL and SST runs could produce similar rainfall patterns with overestimation. Due to the northward shift of landfall location in CNTL and SST runs, the rainfall is also shifted

to the north. As Viyaru is a slow-moving TC, it could produce a lot of rain during landfall over Bangladesh coast even though it made landfall as a CS. As we observe the Figure 11a, the SST runs could produce comparable distribution of rain with the observation than that of CNTL run for Viyaru. Considering Phailin, the TC produced extremely heavy rainfall over Odisha leading to inland floods causing almost 5 deaths (IDR, 2013; Mohanty et al., 2015). Both the experiments showed similar extreme heavy rainfall over coastal regions of Odisha. The synoptic analyses of Phailin indicated that the presence of secondary eyewall over Northern part of Odisha caused extremely heavy rainfall leading to flooding over this area (RSMC report, 2014). The SST run produced heavy rainfall over northern parts of

Odisha (above 21°N) as observed in the TRMM. The more inland rainfall in SST run could be mainly due to realistic estimation of rain bands. Unlike SST run, the CNTL run failed to produce heavy rains over northern parts of Odisha. Therefore, it can be inferred that realistic representation of relative SST gradient could improve TC rainfall which has also been supported by the recent study (Lin et al. 2015).

Along with the qualitative verification, quantitative verification of 24-hour accumulated rainfall has been carried out for landfall day. The quantitative assessment is carried out using two metrics; Heidke Skill Score (HSS) and bias as follows.

$$HSS = \frac{[(H+CN)] - (expected\ correct)}{[N - expected\ correct]} \quad (1)$$

where, expected correct = $[(H + M)(H+F) + (CN + M)(CN + F)]/N$

where

- hit (H)—event forecast to occur, and did occur
- miss(M)—event forecast not to occur, but did occur
- false alarm (F)—event forecast to occur, but did not occur
- correct negative (CN)—event forecast not to occur, and did not occur
- and the total number (N) = (hits + misses + false alarm + correct negative)

It can be defined as (score value – score for the standard forecast)/(perfect score – score for the standard forecast).

$$\text{Bias} = \text{sum(observation-Model)}/\text{length(observation)} \quad (2)$$

The range of the HSS is $-\infty$ to 1. The skill scores are calculated for different rainfall thresholds using IMD gridded daily rainfall observation and presented in Figure 12(b). Recent studies exhibited less skill in rainfall prediction for higher thresholds in real time forecast. For example, Osuri et al. (2012b) presented that the skill of Advanced Research WRF (ARW) model is ~0.2 up to 5 cm and less rainfall thresholds, thereafter the skill decreases at greater rate. In this study, the skill of the model is more than 0.2 up to 14 cm (moderate rain to heavy rain) from both the runs, which infers that the HWRF performs better than the ARW model for rainfall prediction. A recent study by Mohanty et al. (2015) also demonstrated similar results in rainfall prediction. SST runs show better performance in HSS skill score for all the categories of rainfall threshold as compared to CNTL runs. The bias is also less in the case of SST run. Overall analyses indicate that the HSS decreases as rainfall threshold increases. Therefore, it can be concluded that the performance of mesoscale models for extremely heavy rainfall is not satisfactory. However, recent studies demonstrated that the rainfall prediction can be improved through realistic representation of land surface processes (Chang et al. 2009; Niyogi et al. 2006; Osuri et al. 2017b), vortex

initialization and relocation (Mohanty et al. 2015), and assimilation of inner core observations (Dowell et al. 2011; Aksoy et al. 2012, 2013; Osuri et al. 2015).

Figure 12(c) shows the mean radial distribution of rainfall derived from both the runs of all the cases to assess the ability to reproduce the observed radial distribution by the experiments. As observed, the highest rainfall is noticed in and around the eyewall region because of the presence of intense updraft and cloud coverage. As radial distance increases the rainfall quantity decreases (Rodgers 2001). It is to be noted that the rainfall is more in the eyewall region in the case of CNTL run as compared to SST run which can be attributed to the constant and higher SST.

4. Conclusion

The main objective of the present work is to understand the role of incorporation of the SST evolution in the TC life time over the BoB. 3 pre-monsoon and 3 post-monsoon TCs with total of 31 cases including different ICs are simulated using HWRF modeling system to address the goal. The conclusions from the above results and discussions are assembled in this section. In the general practice this change has not been updated during TC integration due to fixed SST configuration. An analysis of SST shows an average variation of 0.4–2°C is noticed in SST. Hence it is critical to update these SST changes.

The experiments show that six hourly update of SST improves the intensity and structure significantly, with marginal improvement in track of the TCs. The analyses of mean error and skill statistics indicate 11% improvement in track and 22% improvement in intensity prediction with SST update. The analyses of CT and AT errors show that the simulated tracks mostly lie to the left of the observed track and the slower movement of the TC respectively. Comparing with earlier studies, the directionality errors of TC movement are reduced by ~50% in CT and ~60% in AT errors. The reduced CT and AT errors in SST run could lead to less landfall position (20%) and time errors (33%). MAE is reduced with an average of 7 knots for forecast hours >72h for SST runs. There is an overall of 46% reduction in intensity bias for SST runs. The study shows maximum benefit of SST update has been seen for longer forecast lengths rather than shorter forecast lengths.

Overall results indicate that the CNTL run, which uses constant SST through the TC life, shows stronger vortex. The SST runs with the modified SST distribution given from RTG-SST eventually produce less intense TC as compared to the CNTL run. The interaction of TC with the ocean during its passage cools down the SST, reducing the flux exchange that inhibits strengthening of the TC. The vertical structure of warm core has been improved in SST run unlike in CNTL, which has significant contribution in intensity evolution. The qualitative and quantitative analysis of 24-hr accumulated rainfall for the landfall day shows overestimation of rainfall in CNTL run in most of

the cases. The SST run could improve the rainfall intensity and spatial distribution. The skill scores HSS and bias indicated that the rainfall simulated by SST run is skillful with high HSS and low bias up to 14 cm. Radial distribution of rainfall of SST run during the landfall day is close to the observed rainfall.

Acknowledgement: The authors gratefully acknowledge Indian National Center for Ocean Information Services (INCOIS), Indo-US Science and Technology Forum New Delhi and DST-INSPIRE for providing financial support to carry out the research work. NCEP is also acknowledged for availing HWRF model. NCAR is acknowledged for providing GFS analysis and forecast fields. The authors deeply acknowledge the India Meteorological Department (IMD) for providing the best track estimations.

References

- Aksoy, A., S. Lorsolo, T. Vukicevic, K.J. Sellwood, S.D. Aberson, F. Zhang, 2012: The HWRF Hurricane Ensemble Data Assimilation System (HEDAS) for high-resolution data: The impact of airborne Doppler radar observations in an OSSE. *Mon. Weather Rev.*, **140**, 1843–1862.
- Aksoy, A., 2013: Storm-relative observations in tropical cyclone data assimilation with an ensemble Kalman filter. *Mon. Weather Rev.*, **141**, 506–522.
- Arakawa, A., and W.H. Schubert, 1973: Interaction of a cumulus cloud ensemble with the large-scale environment, part-I. *Jour. Of Atmo. Sci.*, **31**, 674–701.
- Bao, J-W., J. M. Wilczak, J-K. Choi, and L. H. Kantha, 2000: Numerical simulations of air-sea interaction under high wind conditions using a coupled model: A study of hurricane development. *Mon. Wea. Rev.*, **128**, 2190–2210.
- Bell, M. M., and M. T. Montgomery, 2008: Observed structure, evolution, and potential intensity of category 5 Hurricane Isabel (2003) from 12 to 14 September. *Mon. Wea. Rev.*, **136**, 2023–2046.
- Bhat, G.S., G.A. Vecchi and S. Gadgil, 2004: Sea Surface Temperature of the Bay of Bengal Derived from the TRMM Microwave Imager. *J. Atmos. Oceanic Tech.*, **21**, 1283–1290.
- Bongirwar, V.S., Rakesh V., C.M. Kishtawal: 2011: Impact of satellite observed microwave SST on the simulation of tropical cyclones. *Nat Haz.*, **58(3)**, 929–944.
- Chan, J.C.L., Y. Duan, and L. K. Shay, 2001: Tropical cyclone intensity change from a simple ocean-atmosphere coupled model. *J. Atmos. Sci.*, **58**, 154–172.
- Chang, Hsin-I, A. Kumar, D. Niyogi, U.C. Mohanty, F. Chen and J. Dudhia, 2009: The role of land surface processes on the mesoscale simulation of the July 26, 2005 heavy rain event over Mumbai, India. *Global and Planetary Change*, **67**, 87–103.
- Chen, H., and S. G. Gopalakrishnan, 2015: A study on the asymmetric rapid intensification of Hurricane Earl (2010) using the HWRF system. *J. Atmos. Sci.*, **72**, 531–550.
- Charney, J. G., A. Eliassen, 1964: On the growth of the hurricane depression. *J. Atmos. Sci.*, **21**, 68–75.
- Chen, S., W. Li, Y. Lu and Z. Wen, 2013: Variations of latent heat flux during tropical cyclones over the South China Sea. *Meteorol. Appl.*, **21**, 717–723.
- Dare, R. A., and J. L. McBride, 2011: Sea surface temperature response to tropical cyclones. *Mon. Wea. Rev.*, **139**, 3798–3808.
- Das, Ananda, Y. Rao, V. Tallapragada, Z. Zhang, and S.K. Roy Bhowmik, and A. Sharma, 2015: Evaluation of the Hurricane Weather Research and Forecasting (HWRF) model for tropical cyclone forecasts over the North Indian Ocean (NIO). *Natural Hazards*, **75**. [10.1007/s11069-014-1362-6](https://doi.org/10.1007/s11069-014-1362-6).
- Deo, A., D.W. Ganer and G. Nair, 2011: Tropical cyclone activity in global warming scenario. *Natural Hazards*, **59**, 771–786.
- Dowell, L. J. Wicker, and C. Snyder, 2011: Ensemble Kalman filter assimilation of radar observations of the 8 May 2003 Oklahoma City supercell: Influences of reflectivity observations on storm-scale analyses. *Mon. Wea. Rev.*, **139**, 272–294.
- Dube, S. K., Indu Jain, A. D. Rao and T. S. Murty, 2009: Storm surge modelling for the Bay of Bengal and Arabian Sea. *Nat Hazards*, **51**, 3–27.
- Emanuel, K.A., 1986: An air-sea interaction theory for tropical cyclones. Part I. *J. Atmos. Sci.*, **43**, 585–605.
- Fiorino, M., J. M. Goerss, J. J. Jensen, and E. J. Harrison Jr., 1993: An evaluation of the real-time tropical cyclone forecast skill of the Navy Operational Global Atmospheric Prediction System in the western North Pacific. *Wea. Forecasting*, **8**, 3–24.
- Gao, S., S. Zhai, L. S. Chiu, and D. Xia, 2016a: Satellite air-sea enthalpy flux and intensity change of tropical cyclones over the western North Pacific. *J. Appl. Meteor. Climatol.*, **55**, 425–444.
- Goni, G., and J. Trinanes, 2003: Ocean thermal structure monitoring could aid in the intensity forecast of tropical cyclones. *Eos, Trans. Amer. Geophys. Union*, **84**, 573–580.
- Gopalakrishnan, S., Q. Liu, T. Marchok, D. Sheinin, N. Surgi, R. Tuleya, R. Yablonsky, and Z. Zhang, 2010: Hurricane Weather Research and Forecasting (HWRF) model scientific documentation. L. Bernardet, Ed., NOAA/Earth System Research Laboratory, 75 pp.
- Gray, W. M., 1975: Tropical cyclone genesis. *Atmospheric Sciences*, Paper No. 234. Colorado State University, Fort Collins, p 119.
- Grell, G. A., 1993: Prognostic evaluation of assumptions used by cumulus parameterizations. *Mon. Wea. Rev.*, **121**, 764–787.
- Hong, S. Y., and H. L. Pan, 1996: Nonlocal boundary layer vertical diffusion in a medium-range forecast model. *Mon. Wea. Rev.*, **124**, 2322–2339.
- IDR 2013: <http://nidm.gov.in/PDF/pubs/India%20Disaster%20Report%202013.pdf>
- Janjic, Z. I., 1994: The step-mountain coordinate model: Further developments of the convection, viscous sublayer and turbulence closure schemes. *Mon. Wea. Rev.*, **122**, 927–945.
- Janjic, Z. I., R. Gall, and M. E. Pyle, 2010: Scientific documentation for the NMM solver. NCAR Tech. Note NCAR/TN-4771STR, 54 pp.
- Jullien, S., P. Marchesiello, C. Menkes, J'erieome Lef'evre, N. Jourdain, G. Samson, M. Lengaigne, 2014: Ocean feedback to tropical cyclones: climatology and processes. *Climate Dynamics*, **43**, 9–10.
- Kaplan, J. and M. DeMaria, 2003: Large-Scale Characteristics of Rapidly Intensifying Tropical Cyclones in the North Atlantic Basin. *Weather and Forecasting*, **18**, 1093–1108.
- Kim, H.S., C. Lozano, V. Thallapragada, D. Iredell, D. Sheinin, H. Tolman, V.M. Gerald, J. Sims, 2014: Performance of Ocean Simulations in the Coupled HWRF-HYCOM Model., *J. Atmos. Ocean Tech.*, **31**, 545–559.
- Knaff, J.A. and M. DeMaria, 2006: A multi-platform satellite tropical cyclone wind analysis system. Preprints. In: 14th conference on satellite meteorology and oceanography. American Meteorological Society, Atlanta, GA, CD-ROM, P4.9.
- Lin, I.I., C. H. Chen, I. F. Pun, W. T. Liu and C. C. Wu, 2009: Warm ocean anomaly, air-sea fluxes and the rapid intensification of cyclone Nargis, 2008: *Geo. Phys. Resea. Lett.*, **36**, 3.
- Lin Y., M. Zhao and M. Zhang, 2015: Tropical cyclone rainfall area controlled by relative sea surface temperature. *Nature Communications*, DOI: [10.1038/ncomms759](https://doi.org/10.1038/ncomms759).
- Ma, Z., J. Fei, L. Liu, X. Huang, and X. Cheng, 2013: Effects of

- the cold core eddy on tropical cyclone intensity and structure under idealized air-sea interaction conditions. *Mon. Wea. Rev.*, **141**, 1285–1303,
- Madi RMSC bulletin: <http://www.rsmcnewdelhi.imd.gov.in/images/pdf/archive/bulletins/2013/RMAD.pdf>
- Mandal, M., U.C. Mohanty, P. Sinha and M. M. Ali, 2007: Impact of sea surface temperature in modulating movement and intensity of tropical cyclones. *Nat Hazards*, **41**, 413–427.
- Miller, B.I., 1958: On the maximum intensity of hurricanes. *J Meteor* **15**, 184–195.
- Mohanty, U.C., K.K. Osuri, V. Tallapragada, F.D. Marks, S. Pattanayak, M. Mohapatra, L.S. Rathore, S.G. Gopalakrishnan, Dev Niyogi, 2015: A Great Escape from the Bay of Bengal “Super Sapphire–Phailin” Tropical Cyclone: A Case of Improved Weather Forecast and Societal Response for Disaster Mitigation., *Earth Interactions.*, **19**, 1–11.
- Mohapatra, M., B.K. Bandyopadhyay, D.P. Nayak, 2013a: Evaluation of operational tropical cyclone intensity forecasts over north Indian Ocean issued by India Meteorological Department. *Nat. Haz.*, **68** (2), 433–451.
- Mohapatra, M., D.R. Sikka, B.K. Bandyopadhyay, A. Tyagi, 2013b: Outcomes and challenges of Forecast Demonstration Project (FDP) on landfalling cyclones over the Bay of Bengal. *Mausam*, **64**, 1–12.
- Mohapatra, M., B. Geetha, M. Sharma, 2017: Reduction in uncertainty in tropical cyclone track forecasts over the North Indian Ocean. *Cur. Sc.*, **112** (9), 1826.
- Nadimpalli, R., K. K. Osuri, Sujata Pattanayak, U. C. Mohanty, M. M. Nageswararao, S. Kiran Prasad, 2016: Real-time prediction of movement, intensity and storm surge of very severe cyclonic storm Hudhud over Bay of Bengal using high-resolution dynamical model. *Nat Hazards*, **81**, 1771–1795. DOI [10.1007/s11069-016-2155-x](https://doi.org/10.1007/s11069-016-2155-x).
- Nargis RMSC bulletin: <http://www.rsmcnewdelhi.imd.gov.in/images/pdf/publications/annual-rsmc-report/rsmc-2008.pdf>
- Needham, H. F., B. D. Keim, and D. Sathiaraj, 2015: A review of tropical cyclone-generated storm surges: Global data sources, observations, and impacts. *Rev. Geophys.*, **53**, 545–591. doi:[10.1002/2014RG000477](https://doi.org/10.1002/2014RG000477).
- Niyogi, D., T. Holt, S. Zhong, P.C. Pyle, and J. Basara, 2006: Urban and land surface effects on the 30 July 2003 meso-scale convective system event observed in the southern Great Plains. *J. Geophys. Res.*, **111** (D19).
- Osuri, K.K., U.C. Mohanty, A. Routray and M. Mohapatra, 2012a: The impact of satellite-derived wind data assimilation on track, intensity and structure of tropical cyclones over the North Indian Ocean, *International Journal of Remote Sensing*, **33**(5), 1627–1652.
- Osuri, K.K., U.C. Mohanty, A. Routray, A. M.A. Kulkarni, M. Mohapatra, 2012b: Customization of WRF-ARW model with physical parameterization schemes for the simulation of tropical cyclones over North Indian Ocean. *Nat Hazards*, **63**(3), 1337–1359.
- Osuri, K.K., Mohanty U.C., A. Routray, M. Mohapatra, D. Niyogi, 2013: Real-time track prediction of tropical cyclones over the north Indian Ocean using the ARW model. *J Appl Meteorol Climatol*, **52**, 2476–2492. doi:[10.1175/JAMC-D-12-0313.1](https://doi.org/10.1175/JAMC-D-12-0313.1).
- Osuri, K.K., U.C. Mohanty, A. Routray, Dev Niyogi, 2015: Improved Prediction of Bay of Bengal Tropical Cyclones through Assimilation of Doppler Weather Radar Observations. *Monthly Weather Review*, **143**, 4533–4560.
- Osuri, K.K., R. Nadimpalli, U.C. Mohanty, D. Niyogi, 2017a: Prediction of rapid intensification of tropical cyclone Phailin over the Bay of Bengal using the HWRF modelling system, *Q. J. R. Meteorol. Soc.*, DOI: [10.1002/qj.2956](https://doi.org/10.1002/qj.2956).
- Osuri, K.K., R. Nadimpalli, U.C. Mohanty, F. Chen, M. Rajeevan and D. Niyogi, 2017: Improved prediction of severe thunderstorms over the Indian Monsoon region using high resolution soil moisture and temperature initialization. *Nature Scientific Reports*, **7**, 41377, DOI: [10.1038/srep41377](https://doi.org/10.1038/srep41377).
- Palmen E, 1948: On the formation and structure of tropical hurricanes. *Geophysica*, **3**, 26–38.
- Pattanaik, D.R., Biswajit Mukhopadhyay1, Arun Kumar, 2012: Monthly Forecast of Indian Southwest Monsoon Rainfall Based on NCEP’s Coupled Forecast System, *Atmo. And Clim. Sc.*, **2**, 479–491.
- Phailin RMSC bulletin: <http://www.rsmcnewdelhi.imd.gov.in/images/pdf/archive/bulletins/2013/NPHA.pdf>
- Pothapakula, P.K., K.K. Osuri, S. Pattanayak, U.C. Mohanty, S. Sil and R. Nadimpalli, 2017: Observational perspective of SST changes during life cycle of tropical cyclones over Bay of Bengal. *Natural Hazards*, **88** (3), 1769–1787.
- Riehl, H., 1954: Tropical Meteorology. McGraw-Hill, New York, 392 pp.
- Reynolds, R.W. and D.C. Marsico, 1993: An Improved Real-Time Global Sea Surface Temperature Analysis. *J. Climate*, **6**, 114–119. [https://doi.org/10.1175/1520-0442\(1993\)006<0114:AIRT GS>2.0.CO;2](https://doi.org/10.1175/1520-0442(1993)006<0114:AIRTGS>2.0.CO;2).
- Roano RMSC bulletin: <http://www.rsmcnewdelhi.imd.gov.in/images/pdf/archive/bulletins/2016/RROA.pdf>
- Rodgers, E.B., R.F. Adler, and H.F. Pierce, 2001: Contribution of tropical cyclones to the North Atlantic climatological rainfall as observed from satellites. *J. Appl. Meteor.*, **40**, 1785–1800.
- Sanabria, E., B. Barrett, P.G. Black, S. Chen, J.A. Cummings, 2013: Real-Time Upper-Ocean Temperature Observations from Aircraft during Operational Hurricane Reconnaissance Missions: AXBT Demonstration Project Year One Results. *Weather and Forecasting*, **28**. DOI: [10.1175/WAF-D-12-00107.1](https://doi.org/10.1175/WAF-D-12-00107.1)
- Sandery, P.A., G.B. Brassington, A. Craig, and T. Pugh, 2010: Impacts of ocean-atmosphere coupling on tropical cyclone intensity change and ocean prediction in the Australian region. *Mon. Wea. Rev.*, **138**, 2074–2091.
- Schade, L.R., and K.A. Emanuel, 1999: The ocean’s effect on the intensity of tropical cyclones: Results from a simple coupled atmosphere-ocean model. *J. Atmos. Sci.*, **56**, 642–651.
- Shay, L.K., G.J. Goni, and P.G. Black, 2000: Effects of a warm oceanic feature on Hurricane Opal. *Mon. Wea. Rev.*, **128**, 1366–1383.
- Sidr RMSC bulletin: <http://www.rsmcnewdelhi.imd.gov.in/images/pdf/publications/annual-rsmc-report/rsmc-2007.pdf>
- Srinivas, C.V., D.V. Bhaskar Rao, V. Yesubabu, R. Baskaran and B. Venkatramana, 2013: Tropical cyclone predictions over the Bay of Bengal using the high-resolution Advanced Research Weather Research and Forecasting (ARW) model. *Q. J. R. Meteorol. Soc.*, **139**, 1810–1825.
- Thiébaux, J., E. Rogers, W. Wang, and B. Katz, 2003: A New High-Resolution Blended Real-Time Global Sea Surface Temperature Analysis. *Bull. Amer. Meteor. Soc.*, **84**, 645–656. <https://doi.org/10.1175/BAMS-84-5-645>.
- Viyaru RMSC bulletin: <http://www.rsmcnewdelhi.imd.gov.in/images/pdf/archive/bulletins/2013/RMAHA.pdf>
- Wu, C-C., C-Y. Lee, and I-I. Lin, 2007: The effect of the ocean eddy on tropical cyclone intensity. *J. Atmos. Sci.*, **64**, 3562–3578.
- Yablonsky, R.M., I. Ginis, B. Thomas, V. Tallapragada and D. Sheinin, L. Bernardet, 2015: Description and Analysis of the Ocean Component of NOAA’s Operational Hurricane-Weather Research and Forecasting Model (HWRF). *J. Atmo. And Oceanic Technol.*, **32**, 144–163.
- Zhao, X., Johnny C. L. Chan, 2016: Changes in tropical cyclone intensity with translation speed and mixed-layer depth: idealized WRF-ROMS coupled model simulations. *Q. J. R. Meteorol. Soc.* **143**, 152–163.